AFRL-PR-WP-TR-2005-2190

AEROSPACE POWER SCHOLARLY RESEARCH PROGRAM

Delivery Order 0011: Modeling Lithium-Ion Conducting Channel

Dr. Perla B. Balbuena

Texas A&M University
Department of Chemical Engineering
College Station, TX 77843

DECEMBER 2005

Final Report for 01 October 2002 – 30 September 2004

STINFO FINAL REPORT

PROPULSION DIRECTORATE
AIR FORCE MATERIEL COMMAND
AIR FORCE RESEARCH LABORATORY
WRIGHT-PATTERSON AIR FORCE BASE, OH 45433-7251

NOTICE

Using Government drawings, specifications, or other data included in this document for any purpose other than Government procurement does not in any way obligate the U.S. Government. The fact that the Government formulated or supplied the drawings, specifications, or other data does not license the holder or any other person or corporation; or convey any rights or permission to manufacture, use, or sell any patented invention that may relate to them.

This report was cleared for public release by the Air Force Research Laboratory Wright Site (AFRL/WS) Public Affairs Office (PAO) and is releasable to the National Technical Information Service (NTIS). It will be available to the general public, including foreign nationals.

PAO Case Number: AFRL/WS-05-2417
Date cleared: 19 Oct 2005

THIS TECHNICAL REPORT IS APPROVED FOR PUBLICATION.

//S//

LAWRENCE G. SCANLON, JR.
Program Manager
Power Division

//S//

JOHN NAIRUS
Chief, Electrochemistry &
Thermal Sciences Branch
Power Division

//S//

BRAD BEATTY, Major
Deputy for Science
Power Division

This report is published in the interest of scientific and technical information exchange and its publication does not constitute the Government's approval or disapproval of its ideas or findings.

REPORT DOCUMENTATION PAGE

Form Approved
OMB No. 0704-0188

1. REPORT DATE *(DD-MM-YY)*	2. REPORT TYPE	3. DATES COVERED *(From - To)*
December 2005	Final	10/01/2002 – 09/30/2004

4. TITLE AND SUBTITLE
AEROSPACE POWER SCHOLARLY RESEARCH PROGRAM
Delivery Order 0011: Modeling Lithium-Ion Conducting Channel

5a. CONTRACT NUMBER
F33615-98-D-2891-0011

5b. GRANT NUMBER

5c. PROGRAM ELEMENT NUMBER
62203F

6. AUTHOR(S)
Perla B. Balbuena

5d. PROJECT NUMBER
3145

5e. TASK NUMBER
32

5f. WORK UNIT NUMBER
Z2

7. PERFORMING ORGANIZATION NAME(S) AND ADDRESS(ES)

Texas A&M University
Department of Chemical Engineering
College Station, TX 77843

8. PERFORMING ORGANIZATION REPORT NUMBER

9. SPONSORING/MONITORING AGENCY NAME(S) AND ADDRESS(ES)

Propulsion Directorate
Air Force Research Laboratory
Air Force Materiel Command
Wright-Patterson AFB, OH 45433-7251

10. SPONSORING/MONITORING AGENCY ACRONYM(S)
AFRL/PRPS

11. SPONSORING/MONITORING AGENCY REPORT NUMBER(S)
AFRL-PR-WP-TR-2005-2190

12. DISTRIBUTION/AVAILABILITY STATEMENT
Approved for public release; distribution is unlimited.

13. SUPPLEMENTARY NOTES
Report contains color.

14. ABSTRACT

This report focuses on the development of a lithium-ion conducting channel as a solid-state electrolyte for rechargeable lithium batteries. Dilithium phthalocyanine (Li2Pc) has been used in this development since it can undergo molecular self-assembly to form the ionic ally conducting channel. The essential features of the channel are that it is designed such that the anion matrix of the unsaturated macrocycle forms the channel through which the lithium ions moves, thus making it a single-ion conductor for lithium ions; the ionic transport of lithium depends on the electric field gradient created by the electrodes, thereby minimizing temperature dependence for ionic transport. Part II of this study shows that Li2Pc preferentially aligns with the galleries of the iron sulfide cathode thereby facilitating lithium-ion transfer between the electrolyte and the cathode.

15. SUBJECT TERMS
Solid-state electrolyte, lithium-ion conducting channel, lithium battery, ionic conduction

16. SECURITY CLASSIFICATION OF:			17. LIMITATION OF ABSTRACT:	18. NUMBER OF PAGES	19a. NAME OF RESPONSIBLE PERSON (Monitor)
a. REPORT	b. ABSTRACT	c. THIS PAGE			Lawrence G. Scanlon, Jr.
Unclassified	Unclassified	Unclassified	SAR	28	19b. TELEPHONE NUMBER *(Include Area Code)* (937) 255-2832

Standard Form 298 (Rev. 8-98)
Prescribed by ANSI Std. Z39-18

Table of Contents

Part I: The structure and dynamics of self-assembled di-lithium pthalocyanine (Li_2Pc)…1

I. 1. Introduction……..1

I. 2. Methodology: Molecular dynamics simulations……..3

I. 3. Results and Discussion…….3

I. 3. 1. Structure……3

I. 3. 2. X-ray spectra…….5

I. 3. 3. Ion channel formation and ionic diffusion……...7

Part II: Properties of self-assembled Li_2Pc at the Li_2Pc-pyrite interface……....9

II. 1. Background……....9

II. 2. Simulation details……..10

II. 3. Results and discussion……...12

II.3.1 Initial stacking axis of Li_2Pc self-assembly is perpendicular to the pyrite (100) surface……..12

II.3.2 Initial stacking axis of Li_2Pc parallel to the pyrite (100) surface…….16

II.3.3 Comparison of the total energy……17

III. Conclusions……..18

References……..19

Part I: The structure and dynamics of self-assembled di-lithium pthalocyanine (Li_2Pc)

I. 1. Introduction

Di-lithium phthalocyanine (Li_2Pc), as shown in Figure 1, has been proposed as a solid electrolyte for lithium-ion batteries, with the expected advantage of providing single-ion transport characteristics for lithium ions.[1]

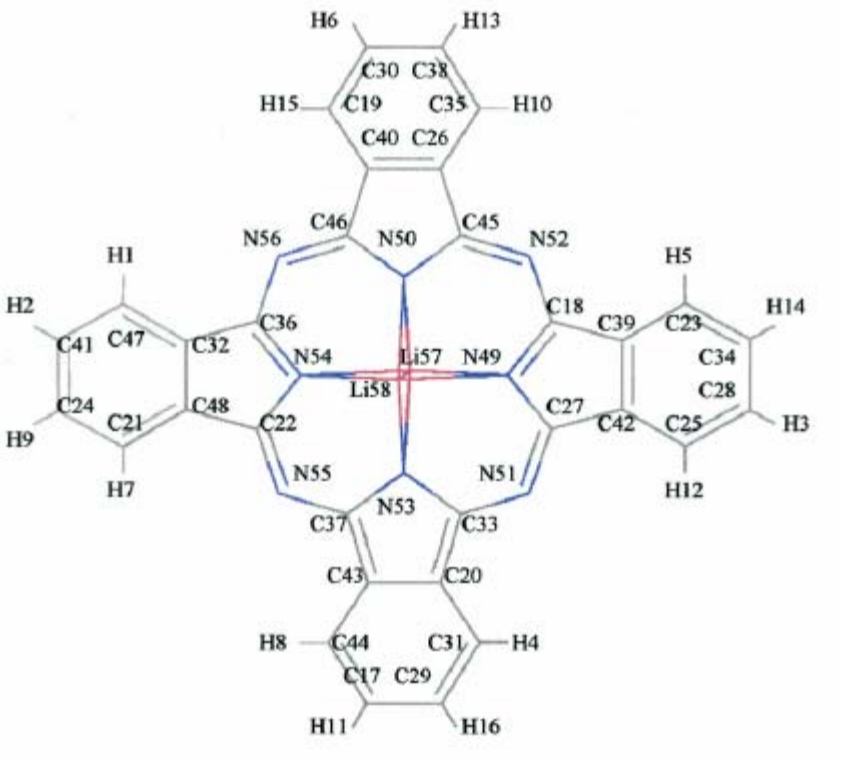

Figure 1: Li_2Pc molecule.

Molecular self-assembly may lead to the formation of lithium ion conducting channels, where the anion matrix of di-lithium phthalocyanine, an unsaturated macrocyclic compound, forms the channel. When such self-assembled structure is used as solid electrolyte of lithium-ion batteries, lithium ion transport may depend on the electric field gradient established between the electrodes, instead of being a function of polymer segmental motion as that observed for oxygen-based solid polymer electrolytes, and therefore, it is expected that the temperature dependence for lithium ion conduction will be minimized. Also, voltage drop across the electrolyte will be minimized even at high current loads because of the single-ion transport characteristics. The performance of Li_2Pc as electrolyte in an all-solid state electrochemical cell has been recently reported.[2]

In view of the potential advantages of the use of Li_2Pc as a solid electrolyte, understanding the lithium-ionic transport mechanisms in solid Li_2Pc becomes essential. However, little is known about its crystalline structure. Other metal phthalocyanines are known to be polymorphic.[3-13] Particularly, a great deal of research has been done on the polymorphism of lithium phthalocyanine because of its potential use as an oximetry probe and its interesting electrical and magnetic behavior.[7,8] Depending on the preparation conditions, LiPc can crystallize in three different structures, namely, α-, β-, and χ-forms. The α- and β-forms of LiPc show monoclinic unit cells with parameters a = 2.57 nm, b = 0.38 nm, c = 2.36 nm, and β = 91.0° and space group C2/c,[14] and a = 1.94 nm, b = 0.49 nm, c = 1.40 nm, and β = 120.36° and space group $P2_{1/c}$,[15] respectively. The χ-form shows a tetragonal unit cell with parameters $a = b$ = 1.385 nm and c = 0.65 nm and the space group P4/mcc.[9] These three polymorphs showed different properties correlated to the nature of molecular packing.[10]

X-Ray spectra of Li_2Pc were obtained at Argonne National Laboratory[16] and at the Air Force Laboratory where Li_2Pc solid state density was also determined.[17] We have used this information to formulate models that, in conjunction with ab initio data for the single molecule and dimers are input for classical molecular dynamics (MD) simulations used to investigate self-assembled structures and determine their corresponding X-Ray spectra. We focused on the characterization of structural and dynamical properties of a self-

assembly of Li_2Pc and its potential to provide lithium-ion conducting channels for lithium-ion batteries. Calculated X-Ray spectra and lithium-ion diffusion coefficients are compared to experimental results. The possibility of existence of ion-channels in the solid state structure is investigated through analyses of configurations derived from the MD simulations.

I. 2. Methodology: Molecular dynamics simulations.

Four primitive unit cells (designated as α-, β-, ε-, and χ-forms) were built based on several sources of data for this and related systems: 1) the analysis of experimental X-Ray spectra of crystalline Li_2Pc,[16](for the ε-form); 2) the experimental density of solid Li_2Pc at room temperature[17] (for the α-, β-, and χ-forms); 3) the reported polymorphism of various metal phthalocyanines[7,8,10] (for the α-, β-, and χ-forms). The cell parameters of the four configurations along with all simulation details have been reported.[18] Among these polymorphs, the α-, β-, and ε-form structures have monoclinic unit cells, and the χ-form has a tetragonal unit cell. The primitive unit cells for the α-, β-, and χ-forms have the same dimensions as the reported structures for the polymorphs of LiPc except that the shortest cell dimension was elongated to fit the experimental density of Li_2Pc (1.40 g/cm^3). The cell parameters of the ε-form were chosen to match the crystal d-spacing that best reproduces the experimental X-Ray data, as calculated with the powder indexing program CRYSFIRE 2002.[19] The DL_POLY program,[20] version 2.13, was used in all simulations. MD simulations were run in the microcanonical ensemble (NVE) for 1200 ps with a time step of 0.001 ps at 300 K. Equilibration runs of 500 ps were performed before collecting averages in production runs of 700 ps. During the equilibration phase, the interval for scaling velocities according to the selected temperature was set to 0.002 ps, in the production phase the scaling is disconnected, but the temperature remains about constant. The cutoff radius, beyond which intermolecular interactions of the real space part of the long-range electrostatic and the van der Waals potentials were set to zero, was chosen as 10.0 Å, which corresponds to half the minimum cell length.

I. 3. Results and Discussion

I.3.1 Structure. The final structures (after 1200 ps total simulation length) of the four forms of Li_2Pc (Table 1) are shown in Figure 2. The corresponding Li-Li intramolecular distance (for α-, β-, ε-, and χ-forms) are also computed as averages and reported in Table

7. The MD results (Figure 2) indicate that molecules in ε-form and χ-form are shifted from each other in two adjacent layers, while those in the α-form and β-form are staggered. In the shifted structure, lithium atoms locate between the ring center of one molecule and one of the benzene rings of the second molecule, whereas in the staggered structure, both lithium atoms locate between the ring centers of the two molecules. The separations between layers have been computed (from the last MD configuration of each case) as averages over measured distances between all the equivalent two adjacent layers within the simulation cell.[18] Comparison of these distances with those of $(Li_2Pc)_2$ calculated by B3LYP/6-31G(d) (3.72 Å for the staggered form and 3.77 Å for the shifted form) indicates good agreement between MD and DFT regarding the staggered forms, whereas shorter distances are found by MD in the shifted configurations.[18]

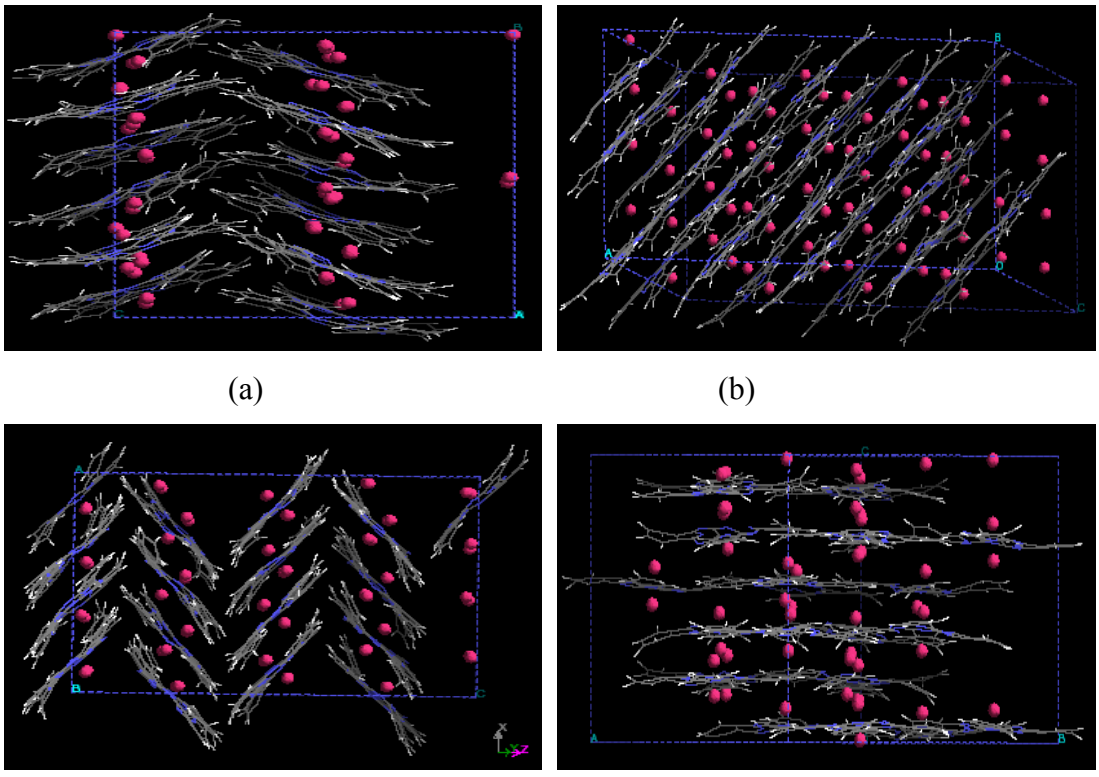

Figure 2: Structures resulting from MD after 1200ps of production time

(a) α-form, (b) β-form, (c) ε-form, (d) χ-form

Another difference between the DFT dimer structures and the MD results arises from the intramolecular distance between two lithium atoms, which are elongated after MD (2.2-2.6 Å for ε-, and χ-forms, and 2.4-2.9 Å for α-, and β-forms), whereas 1.99 Å, 2.23 Å, and 2.56 Å separations were found after B3LYP/6-31G(d) geometry optimization of a single molecule as well as in the shifted and staggered dimers, respectively. The longer Li-Li intramolecular distances obtained from the MD simulations in comparison with the DFT results point to the influence of collective effects of the much larger ensemble of molecules in the MD simulations, but also they may be a reflection of a weakening of the Li-N bonds which would facilitate the mobility of the lithium atoms in the self-assembled structure. On the other hand, the small energy difference found between the average total energies[18] is an indication of possible polymorphism of Li_2Pc.

I.3.2 X-ray spectra. PowderCell Version 1.0,[21] a program for exploring and manipulating crystal structures and calculating X-Ray powder patterns was used to calculate X-Ray spectra corresponding to the simulated structures. This program uses as input primitive cell parameters and structure (atomic positions) and simulates an X-Ray pattern using Bragg's law, weighting the contributions of each atom with calculated structure factors. We used as input the coordinates from the final molecular structure of the MD simulations in the primitive cells of each of the four crystalline forms, along with their respective primitive cell parameters,[18] to obtain simulated X-Ray powder diffractograms.

Figures 3a and b show experimental X-ray diffraction spectra of Li_2Pc synthesized in Argonne National Laboratory (dried at 220 ^oC in vacuum), and received from Aldrich (dried at 160 ^oC in vacuum) respectively. Comparing the two experimental spectra, we observe that in 3a several sharp peaks appear at an angle 2θ around 20^o, but only a broad peak is detected in 3b, where some small peaks disappear. We speculate that the experimental X-ray spectra may reflect a mixture of Li_2Pc polymorphs, some of them less crystalline than others; the presence of impurities may also add new features to the spectrum, as observed in other metal phthalocyanines.[13,22] In addition, different methods to synthesize Li_2Pc may give different mixtures of Li_2Pc polymorphs. It is also possible that structural changes may exist because of the different drying temperatures.

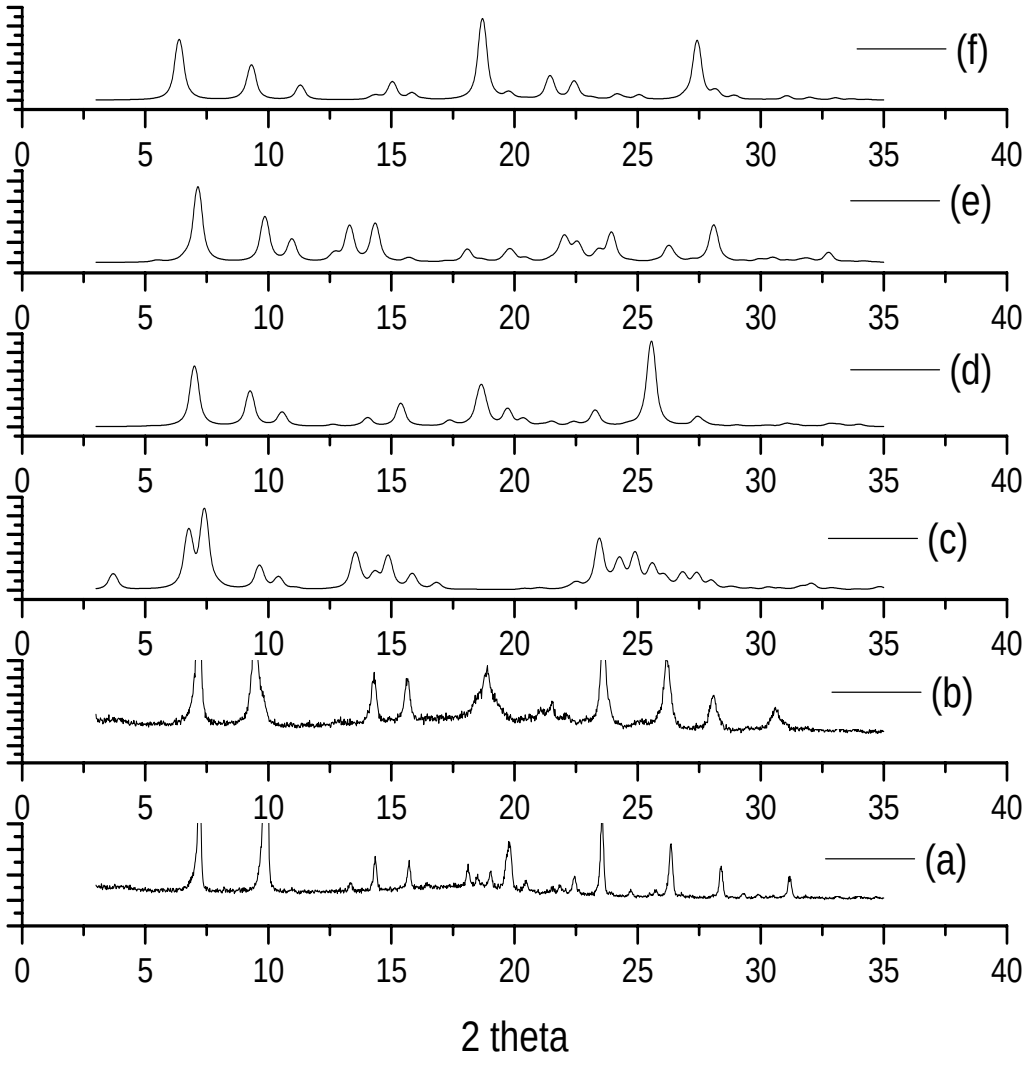

Figure 3: Comparison of simulated X-ray with experimental data
(a) Li_2Pc synthesized in Argonne National Laboratory (dried at 220 ^oC vacuum)
(b) Li_2Pc from Aldrich (dried at 160 ^oC vacuum)
(c) α-form, (d) β-form, (e) ε-form, (f) χ-form

Figures 3c to f show the simulated X-ray spectra for the four investigated crystalline forms. In our comparative analysis, we notice that internal molecular reorientations of the Li_2Pc molecules in a primitive cell may cause enhancement, reduction, or even disappearance of some of the peaks that would arise because of the primitive cell dimensions, and the possible influence of polymorphism in the experimental data may obscure a direct comparison of the calculated and experimental

structures. However, we perform a direct comparison of each of the calculated spectrum to the experimental data (Figs. 3a and b), assuming that the latter are single crystalline phases.

A reasonable agreement in the peak positions is found for the ε-form (Figure 3e), not surprisingly since the parameters of the primitive cell of the ε-form were selected to reproduce the d-spacing of the experimental diffractogram of Figure 3a; however the agreement is less satisfactory for angles $2\theta > 20^{o}$. The correspondence is much better for the β-form which has similar dimensions to the ε-cell. Moreover, comparison between the relative intensities of the simulated diffraction peaks with the experimental ones, points to a better agreement of the β-form over the ε-form. The experimental spectra in Figures 3a and b, and that of the calculated β-phase (Figure 3d) show also a close similarity to the reported spectra for the β-phase of H_2Pc[22] and MgPc.[13]

On the other hand, the simulated X-ray spectrum of the α-form of Li_2Pc exhibits few and rather broad diffraction peaks, compared to other three Li_2Pc simulated polymorphs. This feature is indicative of a low crystallinity of the α-form, which was also observed for the α-forms of other metal phthalocyanines.[7,23] The fusion of the two peaks appearing in the range $5 < 2\theta < 10^{o}$ is another characteristic of the α–phase, also detected in other metal and non-metal phthalocyanines.[13,22] In comparison with Figures 3a and b, we discard the contribution of the α-phase to the experimental spectrum.

The simulated X-ray spectrum of the χ-form shows a well defined crystalline structure. However, although some peaks appear at the same position of the experimental ones, most of them do not, and probably the χ-form is not the predominant form that contributed to the experimental data. However, the peak of highest intensity for this structure appears a value 2θ of 18.8^{o} in coincidence with the broad peak of Figure 3b that makes the main difference between the experimental structures Figures 3a and b. This aspect points out to the possibility of a mixture of the most-likely β-form with the χ-form in the experimental (Figure 3b) spectrum. In summary, the results in Figure 3 indicate that the best agreement between experimental and calculated results is found for the β-phase.

I.3.3 Ion channel formation and ionic diffusion. Looking at the self-assembly molecular organization, an alignment of lithium ions is found that can be associated with the

expected lithium ion conducting channels. We can visualize these conducting channels in α-form, β-form, and ε-form when combining the top (not shown) and side views of the unit cells,[18] or rotating the unit cell of χ-form. These chains of ions are oriented along the same direction across layers.

To investigate lithium mobility, we calculated the velocity autocorrelation function (VAF), which is related to the macroscopic, phenomenological, self-diffusion coefficient *D* through the Green-Kubo formula,[24] written as the time integral of a microscopic time-correlation function:

$$D = \int_0^\infty \left\langle v(t).v(t_0) \right\rangle_{t_0} dt \qquad (1)$$

where the function in brackets is a measure of the projection of the particle velocity at time t onto its initial value, averaged over all initial conditions t_0. The velocity autocorrelation function of lithium ions shows oscillations in the time domain, indicating the rattling motion of lithium ions in the "cage" of their nearest neighbors.[18] The corresponding conductivity of lithium ions was calculated via the Nernst-Einstein equation,

$$\kappa = \frac{cDz^2F^2}{RT} \qquad (2)$$

where the *c* is the concentration of lithium ions, *D* is the ionic diffusion coefficient, *z* is the charge on lithium ions, *F* is the Faraday constant, *R* is the gas constant, and *T* is the absolute temperature.

Table 1: **Calculated diffusion coefficient and conductivity of lithium ions in various Li_2Pc crystalline forms at 300K.**

Li_2Pc crystalline form	Diffusion coefficient (cm^2/s)	Conductivity* (S/cm)
α	5.94×10^{-9}	2.65×10^{-5}
β	1.35×10^{-8}	6.03×10^{-5}
ε	2.04×10^{-8}	9.79×10^{-5}
χ	1.88×10^{-8}	8.40×10^{-5}

*Experimental ionic conductivities of 5.1 to 8.9 $\times10^{-4}$ S/cm were obtained at 300 K.[17]

The results shown in Table 1 illustrate the differences in ionic mobility imposed by the various crystal structures, with the less crystalline α-form having the smallest self-diffusion coefficient and the ε-form the highest. A transport mechanism for lithium ions in Li_2Pc has been suggested, whereby instead of depending on polymer segmental motion as in the PEO system,[25] the lithium ion diffusion would depend mainly on the electric field gradient in the system. Values of diffusion of lithium ions in PEO/$LiClO_4$ mixtures were reported to be 5.2 x 10^{-9} cm^2/s at 349 K,[26] which are below our calculated values at 300 K. Compared to the experimental ionic conductivity in Li_2Pc (Table 1), the simulated lithium ion conductivity results are about one order of magnitude smaller. This difference is explained considering that in the simulation ions move via self-diffusion determined by the field created by the self-assembly of Li_2Pc molecules, while in the experiment diffusion across the electrolyte/electrode interface is driven by a difference of chemical potential and by an electric field gradient established between the electrodes of an electrochemical cell. Work to incorporate the effect of an electric field in the simulations is in progress, and will be reported elsewhere. Further, we note that equation (1) has the implicit assumption that ions at low concentrations do not interact with each other and therefore their motion is uncorrelated. However, this is an oversimplification of this system that has a strong long-range Coulombic component. A more accurate equation would relate the conductivity to the charge flux autocorrelation function,[27] where the charge flux is calculated by the sum of charge times velocity for each ion. Alternatively, one could calculate Maxwell-Stefan diffusion coefficients, where the mass fluxes are linearly related to the gradient of chemical potential instead of being proportional to the gradient of concentration.[28]

Part II: Properties of self-assembled Li_2Pc at the Li_2Pc-pyrite interface

II. 1. Background

The crystalline structure and self-assembly characteristics of di-lithium phthalocyanine were investigated in the first part of our work. However, since lithium ions diffuse from the electrolyte to the electrode, a good interfacial contact is essential. For pyrite cathodes, a thin film of Li_2Pc is grown over the surface of pyrite. Pyrite has a simple cubic structure with space group Pa3 and a unit cell with length parameter of 5.4281 Å

containing four FeS_2 units define this system. Figures 4a and b show the bulk pyrite and pyrite (100) surface. In bulk pyrite, each Fe is coordinated by 6 S atoms and each S by 3 Fe atoms and 1 S atom. In the (100) surface, Fe is coordinated by 5 S atoms; S by 2 Fe atoms and 1 S atom.

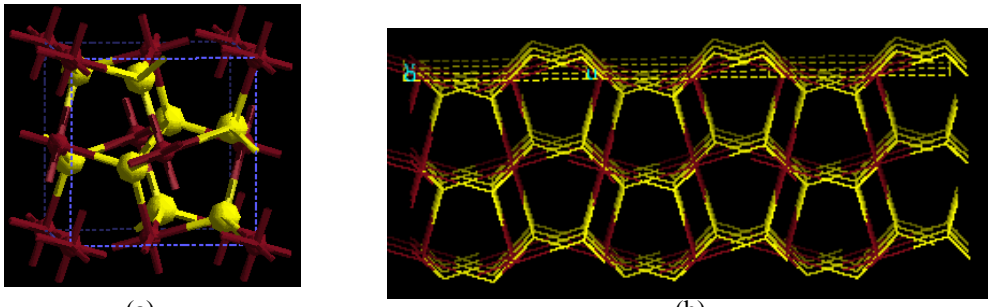

(a) (b)

Figure 4: Structural models of bulk pyrite (a), and pyrite (100) surface (b). The yellow spheres are the S atoms, and the red ones are the Fe atoms.

We use molecular dynamics simulations to analyze the pyrite/Li_2Pc solid-solid interface, with the aim of obtaining structural details of a self-assembled Li_2Pc electrolyte film in contact with a pyrite cathode surface. Also, we try to understand the solid-solid interfacial contact between Li_2Pc and the pyrite surface and investigate the effect of the presence of the pyrite cathode on the formation of the lithium-ion conduction channels in the Li_2Pc phase. By investigating the interfacial structure of the system, several structural and dynamical properties are analyzed, including the radial distribution functions, and adsorption of Li_2Pc on the pyrite (100) surface.

II. 2. Simulation details

The simulation system consists of a 5-layer slab of a pyrite exposing a (100) surface in contact with a mono-layer, a bi-layer, or multi-layers of Li_2Pc located in a tetragonal unit cell, which is subjected to periodic boundary conditions. The 5-layer slab of pyrite contains 250 FeS_2. During the simulation, the pyrite atoms in the slab are fixed. The atomic charges of +0.64 for Fe, and –0.32 for S atoms were taken from published results. The van der Waals force field parameters were taken from the literature.[29] The simulation cell has dimensions of 50.00 Å × 27.14 Å × 27.14 Å.

So far, the initial configuration of Li_2Pc in contact with pyrite (100) surface is of the χ-form previously proposed.[18] Two initial orientations of the χ-form Li_2Pc were studied, where the stacking axis of the self-assembled Li_2Pc is either perpendicular or parallel to the pyrite (100) surface respectively. For initial configurations with stacking axis perpendicular to the surface, 5 cases with systems containing 1, 2, 4, 8, and 16 Li_2Pc were simulated. The Li_2Pc molecules are arranged in layers parallel to the surface, with a maximum number of four Li_2Pc molecules in each layer. Figure 5 shows the initial configuration of the pyrite slab with 4 Li_2Pc molecules in contact with the surface, with an initial separation of 2.5 Å between the Pc ring and the surface.

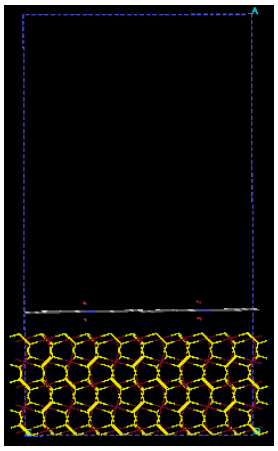

Figure 5. Initial configuration of the pyrite slab with 4 Li_2Pc molecules (a monolayer) in contact with the pyrite (100)

For the cases containing one and two Li_2Pc molecules the separation distance from the surface is kept the same. For the cases contain 8 and 16 Li_2Pc molecules, additional layer (s) were added to the top of the first layer shown in Figure 5, with separation of 3.25 Å between Pc rings. For the simulations where the stacking axis of the self-assembled Li_2Pc was parallel to the pyrite (100) surface, four cases with systems containing 1, 2, 8, and 16 Li_2Pc molecules were simulated. Figure 6a shows the top view of the initial configuration of the pyrite slab in contact with a self-assembly of 8 Li_2Pc molecules covering one half of the pyrite (100) surface. Figures 6 (b), (c), and (d) show the systems containing 1, 2, and 16 Li_2Pc.

The DL_POLY program,[20] version 2.13, was used in all MD simulations. MD simulations were run in the microcanonical ensemble (NVE) for 800 ps with a time step of 0.001 ps. Equilibration runs of 300 ps were performed before collecting averages in production runs of 500 ps. During the equilibration phase, the interval for scaling of velocities according to the selected temperature was set to 0.002 ps; in the production phase the scaling is disconnected, but the temperature remains about constant. The cutoff radius, beyond which intermolecular interactions of the real space part of the long-range electrostatic and the Van der Waals potentials were set to zero, was chosen as 10.0 Å.

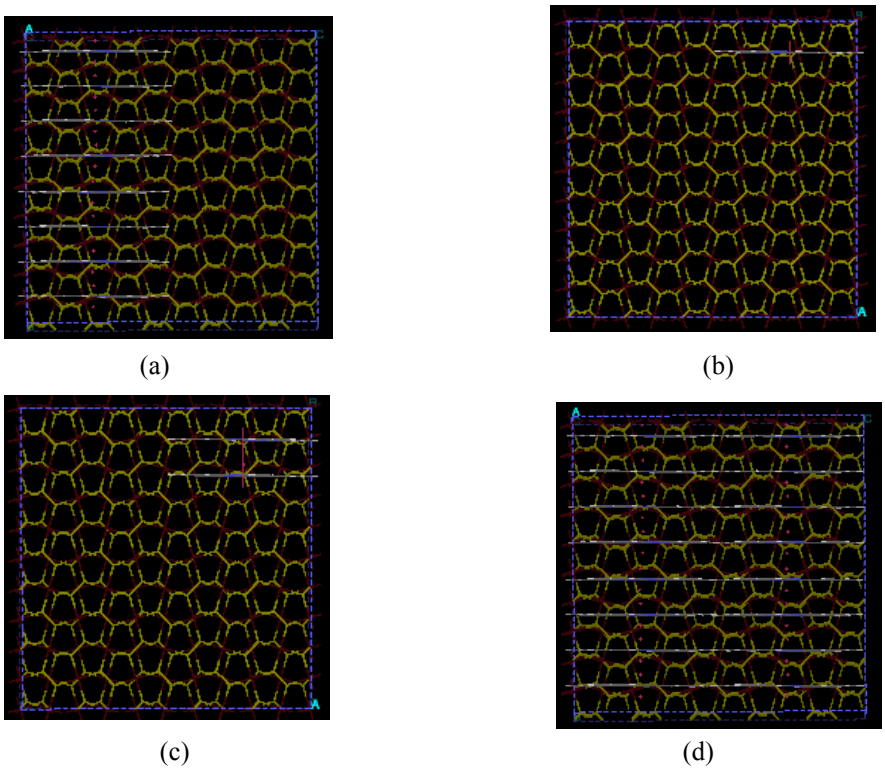

Figure 6: the initial configuration of pyrite slab with stacking axis of Li_2Pc parallel to (100) surface: (a) 8 Li_2Pc, (b) 1 Li_2Pc, (c) 2 Li_2Pc, (d) 16 Li_2Pc

II. 3. Results and discussion

II.3.1 Initial stacking axis of Li_2Pc self-assembly is perpendicular to the pyrite (100) surface

Figure 7 shows the side view of the final configurations of systems with various film thicknesses of Li_2Pc. Compared to the initial separation distance between the Pc ring and the (100) surface, the mean separation distance increased from 2.5 Å to 3.5 Å after the system equilibrates. This is because of the main interactions between pyrite and Li_2Pc, i.e., the electrostatic attraction between Fe and N, Li and S, Li and N, as well as the repulsion between Fe-Li, S-N, and Li-Li. For the systems containing more than one Li_2Pc molecule, shifted dimers were formed.

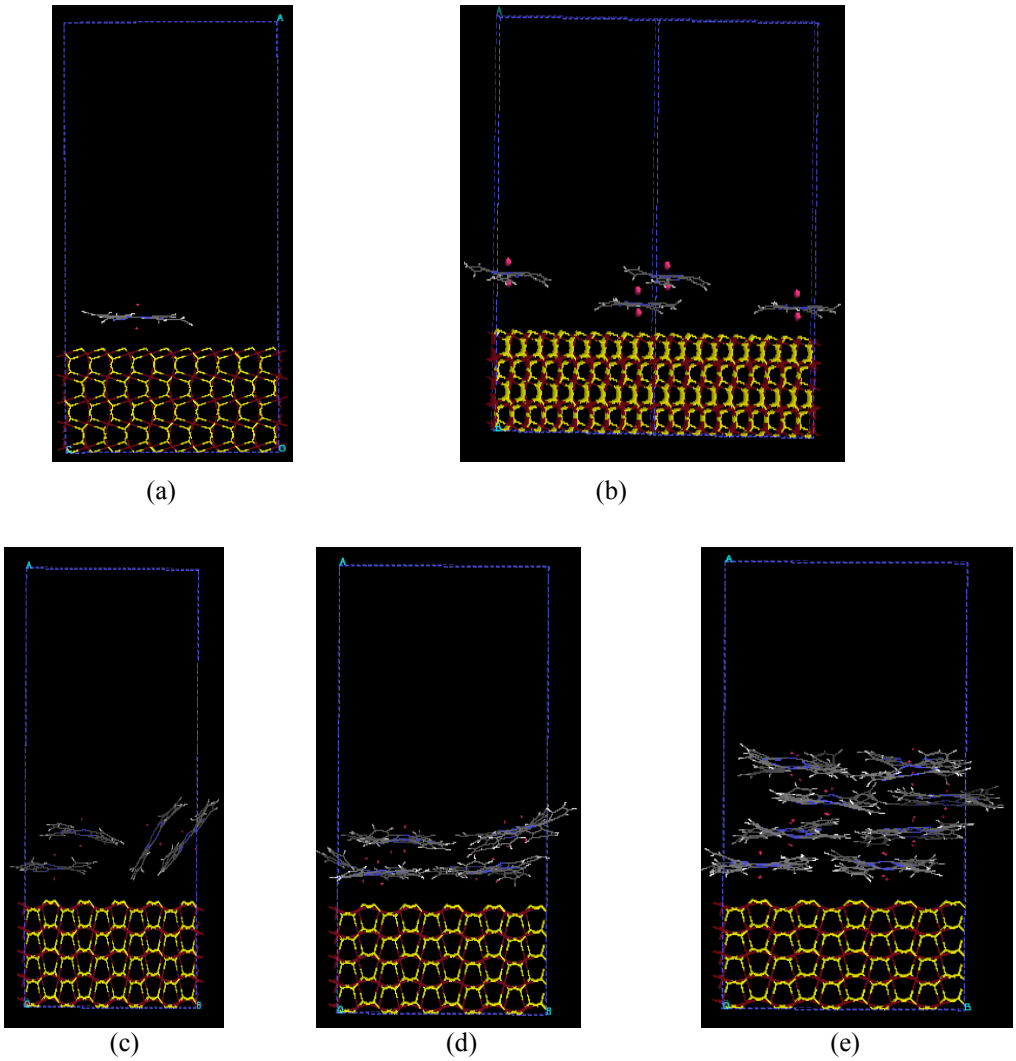

Figure 7: Final configuration of systems with stacking axis of Li_2Pc perpendicular to the pyrite (100) surface with varying number of molecules in the simulation cells: (a) 1 Li_2Pc, (b) 2 Li_2Pc, (c) 4 Li_2Pc, (d) 8 Li_2Pc, (e) 16 Li_2Pc

Figure 7 (b) shows two neighbor cells, illustrating the formation of the shifted dimer. Clearly, we can observe that the system with higher Li_2Pc density retains the χ-form of the Li_2Pc crystalline structure. From the top view in Figures 8a to d, we can see that the lithium ions which are closest to the pyrite (100) surface are adsorbed on sites close to the top of S atoms. It is understandable that lithium ions are not exactly on the top of S atoms, considering the site of Li_2Pc molecule and thus the overall repulsion and attraction interactions between different ion pairs mentioned previously. For example, the location of Li-ions are mainly decided by the interactions of Li-Li, Li-Fe, Li-S, and Li-N. As the number of Li_2Pc molecules increases in the system up to 16 (where the film is composed

of four layers), we begin to see the existence of potential lithium ion conducting channels that were observed in our previous work of bulk self-assembled Li_2Pc.[18] Figure 8 (e) shows such potential conducting channels in four unit cells.

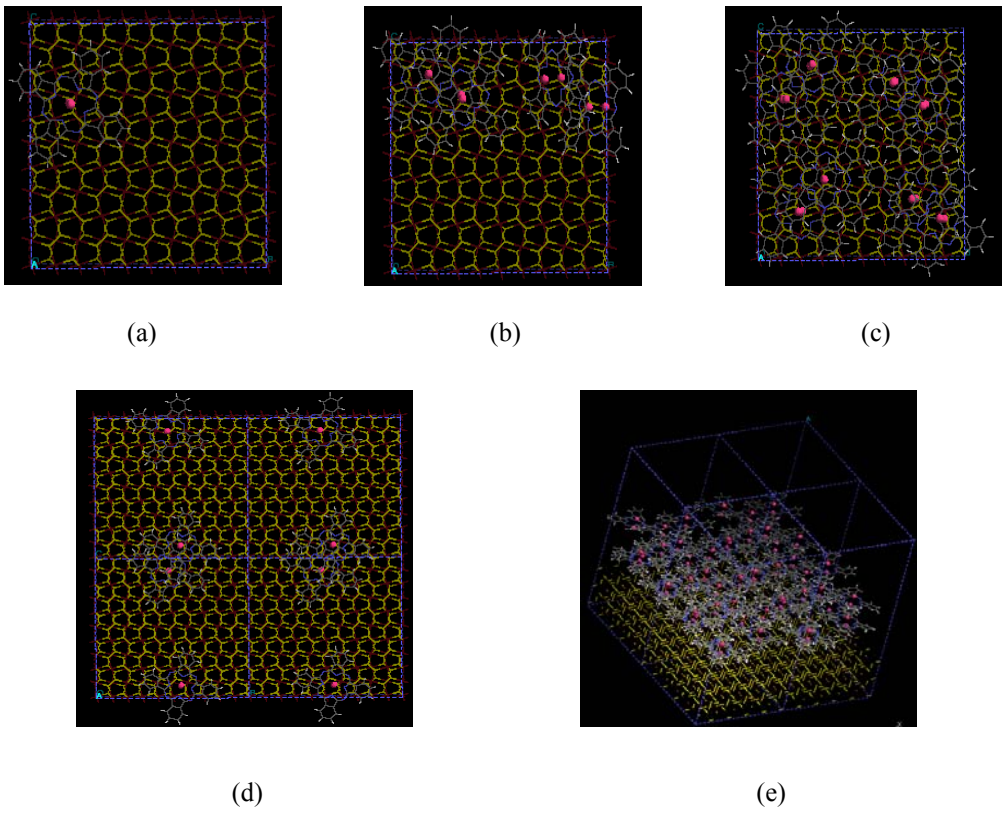

Figure 8 (a) to (d): Top view of final configurations of the system with 1 to 8 Li_2Pc molecules; (e) view of potential lithium ion conducting channels of the system with 16 Li_2Pc molecules. For better visualization, lithium ions are highlighted.

Figures 9 (a) and (b) show the radial distribution functions of Li-S and Fe-N. A sharp first peak in Figure 9 (a) indicates a strong interaction between the Li ions and the S atoms from the surface. The average shortest distance is 2.65 Å. The decrease of the first peak magnitude is due to the relatively smaller atomic fraction of Li atoms on the surface as the Li_2Pc density increases. The position of the first peak shifts to the left as the density of Li_2Pc increases, indicating enhanced S-Li interactions. The negatively charged N atoms of Li_2Pc interact with the positively charged Fe atoms of the substrate; however, the shortest distance Fe-N is larger than 4 Å, showing that the molecule attaches to the surface via the Li-S interaction.

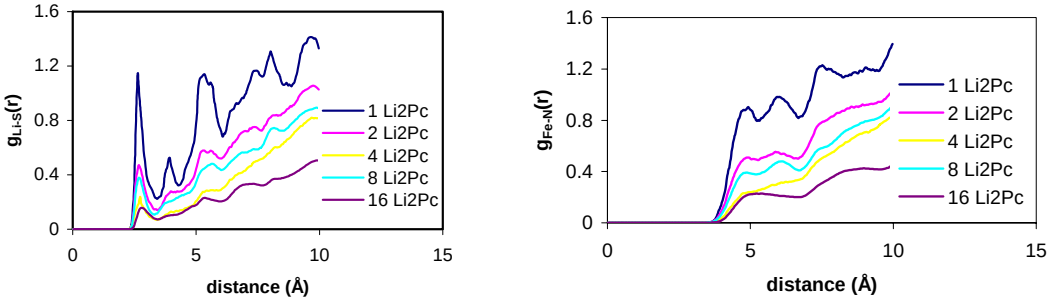

Figure 9: Radial distribution function of initial Li_2Pc stacking axis perpendicular to pyrite (100) surface, (a) Li-S, (b) Fe-N

In order to test the formation of shifted Li_2Pc dimers above the pyrite surface is not caused by the small pyrite (100) surface contacted with Li_2Pc, we used another 5 layer pyrite slab with $(FeS_2)_{640}$ and 4 Li_2Pc. The pyrite (100) surface has dimensions of 43.42 Å × 43.42 Å. Initially, four Li_2Pc were located on the same plane parallel to the pyrite (100) surface, with a separation distance of 2.5 Å between each Pc ring and the surface. Compared to previous systems, the surface has a much larger area than that occupied by the four Li_2Pc molecules. Figure 10 shows the final configuration of the system. The final configuration indicated that one of the Li_2Pc molecules moved away from the surface and formed a second layer.

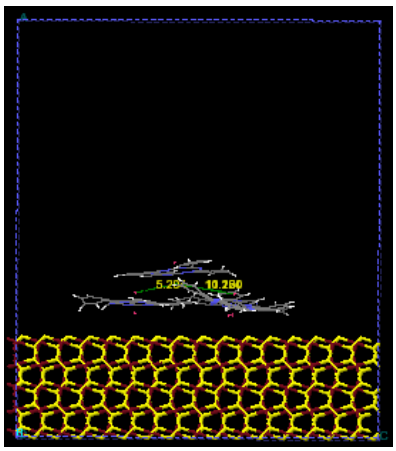

Figure 10: $(FeS_2)_{640}$ with 4 Li_2Pc

By checking the distance from the Li ions belonging to two Li_2Pc molecules in two different layers, it was found that one pair had the value of 5.28 Å, which corresponded to the intermolecular Li-Li distance of the shifted dimer. Other two Li-Li pairs were more than 10 Å away. The result shows that the formation of shifted dimer is favorable and stable. The formation of the shifted dimer is energetically favorable according to DFT calculations as well.[18]

II.3.2 Initial stacking axis of Li_2Pc parallel to the pyrite (100) surface

Recent studies[30] have found that most dilithium octacyanophthalocyanine [$Li_2Pc(CN)_8$] molecules in the Langmuir-Blodgett film were stacked in a face-to-face aggregated state with stacking axis parallel to a ITO surface. Figures 11 (a) through (d) show the final configurations of the systems with initial stacking axis of Li_2Pc parallel to the pyrite (100) surface, with 1, 2, 8, and 16 Li_2Pc molecules respectively.

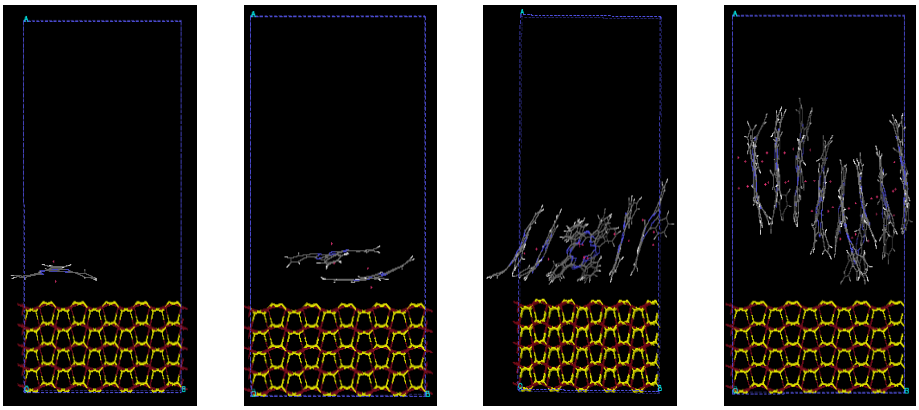

Figure 11: Final configuration of systems with initial stacking axis of Li_2Pc parallel to the pyrite (100) surface, (a) 1 Li_2Pc, (b) 2 Li_2Pc, (c) 8 Li_2Pc, (d) 16 Li_2Pc

For the systems containing one or two Li_2Pc, the final configurations show that the whole ring of Li_2Pc rotated and the stacking axis of the self-assembled system changed from the parallel to the perpendicular position. This is due to the strong interaction between Li and S atoms, as well as to the available free space for Li_2Pc molecules to rotate. This, on the other hand, indicates that the configuration with stacking axis of Li_2Pc perpendicular to the pyrite (100) surface is more stable. Also, we clearly observed the formation of a shifted Li_2Pc dimer for the system with two Li_2Pc molecules. However, for the systems containing 8 and 16 Li_2Pc, we did not observe the rotation of the stacking axis from parallel position to perpendicular position. Li_2Pc molecules in the system with 8 Li_2Pc did rotate a little bit and the Pc rings were no longer completely perpendicular to the pyrite surface, but with an edge-on configuration on the pyrite surface. The configuration of Li_2Pc in this system is similar to the β-form crystalline structure we proposed previously.[18] For the system containing sixteen Li_2Pc molecules, the Pc rings of the final

configuration were relatively perpendicular to the pyrite surface. Although the strong interaction between Li ions and S ions would make the rotation of Li_2Pc, the unavailable free space was the main reason that Li_2Pc could not rotate since the size of Li_2Pc is relatively large. The final configuration of Li_2Pc in this system was the χ-form crystalline structure.

As we mentioned above that the final configurations of systems with 1 and 2 Li2Pc molecules were very similar to the systems with the systems of initial stacking axis of Li2Pc perpendicular to pyrite surface. Figures 12 (a) and (b) show the radial distribution functions of Li-S and Fe-N, respectively.

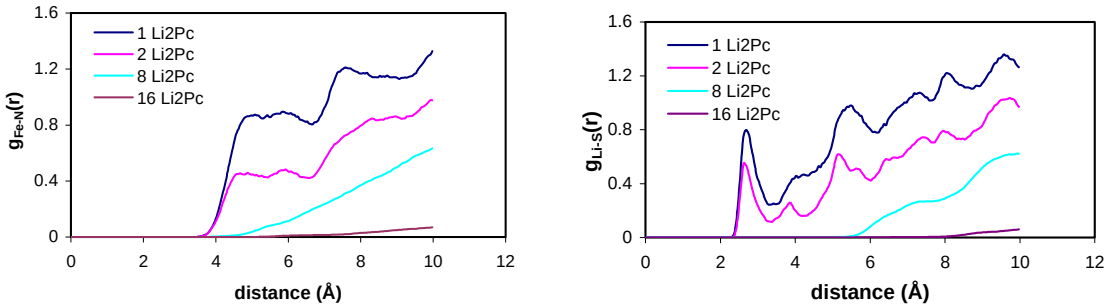

Figure 12: Radial distribution function of initial Li_2Pc stacking axis parallel to pyrite (100) surface, (a) Li-S, (b) Fe-N

From Figure 12 (a), we can see that the average position of the Li-ions with respect to the S atoms on the surface remains equal to 2.65 Å for the cases with 1 and 2 molecules. At higher densities of Li_2Pc, the number of molecules in contact with the surface is significantly reduced, revealing a clear change in the interfacial configuration of the Li_2Pc assembly. The N atoms interact with the Fe atoms with shortest distances found at about 4.5 Å in Figure 12 (b), again we observe the change in configuration as the Li_2Pc density increases.

II.3.3 Comparison of the total energy

Table 2 shows the comparison of the total energy for the various systems. At constant Li_2Pc density, the energies of the various final configurations are only slightly favorable to the case where the stacking axis is perpendicular to the surface, probably because it

maximizes the Li-S and Fe-N interactions. But the small energy difference suggests the possible existence of polymorphic structures.

Table 2: Comparison of total energy (kcal/mol unit cell)

Number of Li_2Pc	Initial stacking axis position to surface	
	Perpendicular	Parallel
1	-8.0796×10^3	-8.0648×10^3
2	-8.4809×10^3	-8.5448×10^3
8	-1.1038×10^4	-1.1059×10^4
16	-1.4608×10^4	-1.4531×10^4

III. Conclusions

Ab initio and molecular dynamics calculations[18] showed the viability of using a large array of molecules to form a lithium ion conducting channel via molecular self-assembly. The elongation of the Li-Li intramolecular distances based on the molecular dynamics calculations illustrate collective effects provided by the self-assembled structure and their importance for facilitating fast ionic transport within the channel.

The close values of the calculated binding energies (B3LYP/6-31G(d)) for the staggered and shifted dimer structures suggest the ease of formation of various polymorphs simultaneously during material preparation, although from the comparison of the simulated and experimental X-Ray data we conclude that Li_2Pc is in a predominant β-phase. On the other hand, calculated ionic conductivities are one order of magnitude below the experimental values, which is primarily attributed to the absence of an external driving force for ionic diffusion in the simulated self-assembled structures.

Molecular dynamics simulations indicate the possibility of existence of possible polymorphic structures of Li_2Pc over the pyrite (100) surface. Energetically, structures with the stacking axis perpendicular to the surface are favorable, although the difference is not significant. In the cases of final configurations of Li_2Pc with a stacking axis perpendicular to the pyrite (100) surface, Li ions are adsorbed over the S ions on the pyrite (100) surface. The interaction between Li ions and S ions increase as the number of the Li_2Pc over the surface increases. At low density of Li_2Pc, shifted dimers are favorable

and more stable. As the density increases, both β- and χ-form structures are found in different systems with 8 Li_2Pc. At high Li_2Pc density, only the χ-form structure is found. Also, the potential lithium ion conducting channels can be realized at high density.

References

(1) Scanlon, L. G.; Lucente, L. R.; Feld, W. A.; Sandi, G.; Campo, D.; Turner, A.; Johnson, C.; Marsh, R. Lithium-ion conducting channel. In *Proceedings of the International Workshop on Electrochemical Systems*; Landgrebe, A. R., Klingler, R. J., Eds., 2000; Vol. 36; pp 326.

(2) Scanlon, L. G.; Lucente, L. R.; Feld, W. A.; Sandi, G.; Balbuena, P. B.; Alonso, P. R.; Turner, A. Composite cathode with Li_2Pc, *J. Electrochem. Soc.* **2003**, submitted.

(3) Fischer, M. S.; Templeton, D. H.; Zalkin, A.; Calvin, M. Structure and Chemistry of the Porphyrins. The Crystal and Molecular Structure of the Monohydrated Dipyridinated Magnesium Phthalocyanin Complex, *J. Am. Chem. Soc.* **1971**, *93*, 2622.

(4) Diel, B. N.; Inabe, T.; Lyding, J. W.; K. F. Schoch, J.; Kannewurf, C. R.; Marks, T. J. Cofacial Assembly of Partially Oxidized Metallomacrocycles as an Approach to Controlling Lattice Architecture in Low-Dimensional Molecular Solids. Chemical, Structural, Oxidation State, Transport, Magnetic and Optical Properties of Halogen-Doped [M(phthalocyaninato)O]n Macromolecules, Where M=Si, Ge, and Sn, *J. Am. Chem. Soc.* **1983**, *105*, 1551.

(5) Dirk, C. W.; Inabe, T.; K. F. Schoch, J.; Marks, T. J. Cofacial Assembly of Partially Oxidized Metallomacrocycles as an Approach to Controlling Lattice Architecture in Low-Dimensional Molecular Solids. Chemical and Architectural Properties of the "Face-to-Face" Polymers [M(phthalocyaninato)O]n Where M=Si, Ge, and Sn, *J. Am. Chem. Soc.* **1983**, *105*, 1539.

(6) Sugimoto, H.; Mori, M.; Masuda, H.; Taga, T. Synthesis and molecular structure of a lithium complex of phtalocyanine radical, *J. Chem. Soc., Chem. Commun.* **1986**, 962.

(7) Brinkmann, M.; Chaumont, C.; Wachtel, H.; Andre, J. J. Polymorphism in powders and thin films of lithium phthalocyanine. An X-Ray, optical and electron spin resonance study, *Thin Solid Films* **1996**, *283*, 97.

(8) Andre, J. J.; Brinkmann, M. Molecular semiconductors for magnetometry and oximetry: lithium phthalocyanine radical, *Synthetic Metals* **1997**, *90*, 211.

(9) Brinkmann, M.; Turek, P.; Andre, J. J. EPR study of the x,a and b structures of lithium phthalocyanine, *J. Mat. Chem.* **1998**, *8*, 675.

(10) Ilangovan, G.; Zweier, J. L.; Kuppusamy, P. Electrochemical Preparation and EPR Studies of Lithium Phthalocyanine: Evaluation of the Nucleation and Growth Mechanism and Evidence for Potential-Dependent Phase Formation, *J. Phys. Chem. B* **2000**, *104*, 4047.

(11) Kimura, T.; Sumimoto, M.; Sakaki, S.; Fujimoto, H.; Hashimoto, Y.; Matsuzaki, S. Electronic structure of lithium phthalocyanine studied by ultraviolet photoemission spectroscopy, *Chem. Phys.* **2000**, *253*, 125.

(12) Yanagi, H.; Manivannan, A. Epitaxial growth of molecular magnetic thin films of lithium phthalocyanine, *Thin Solid Films* **2001**, *393*, 28.

(13) Janczak, J.; Kubiak, R. X-ray single crystal investigations of magnesium phthalocyanine. The 4+1 coordination of the Mg ion and its consequence, *Polyhedron* **2001**, *20*, 2901.
(14) Wachtel, H.; Wittmann, J. C.; Lotz, B.; Petit, M. A.; Andre, J. J. Anisotropic spin transport in oriented lithium phthalocyanine thin films, *Thin Solid Films* **1994**, *250*, 219.
(15) Homborg, H.; Teske, C. L. Lithium phthalocyanines: preparation and characterization of the monoclinic and tetragonal modifications of LiPc(1-) and the halogen adducts LiPc(1-)X (X = Cl, Br, I), *Zeitschrift fuer Anorganische und Allgemeine Chemie* **1985**, *527*, 45.
(16) Johnson, C., Private communication.
(17) Scanlon, L. G., Private communication.
(18) Zhang, Y.; Alonso, P. R.; Martinez-Limia, A.; Scanlon, L. G.; Balbuena, P. B. Crystalline structure and lithium-ion channel formation in self-assembled di-lithium phtalocyanine: Theory and experiments, *J. Phys. Chem. B* **2003**, *108*, 4659.
(19) Shirley, R. The CRYSFIRE System for Automatic Powder Indexing: User's Manual, The Lattice Press Guildford, Surrey GU2 7NL, England, 2000.
(20) Smith, W.; Forester, T. R. DL_POLY; Daresbury Laboratory: Daresbury, 1996.
(21) Kraus, W.; Nolze, G. PowderCell for Windows; Federal Institute for Materials Research and Testing: Berlin, Germany, 1997.
(22) Kubiak, R.; Janczak, J.; Ejsmont, K. On polymorphic and non-polymorphic conversions of phthalocyanines, *Chem. Phys. Lett.* **1995**, *245*, 249.
(23) Assour, J. M.; Harrison, S. E. Electron spin resonance of concentrated copper phthalocyanine crystals., *Physical Review* **1964**, *136*, 1368.
(24) Hansen, J.-P.; McDonald, I. R. *Theory of simple liquids*, 2nd. ed.; Academic Press: San Diego, CA, 1990.
(25) Kuppa, V.; Manias, E. Computer Simulation of PEO/Layered-Silicate Nanocomposites: 2. Lithium Dynamics in PEO/Li+ Montmorillonite Intercalates, *Chem. Mater.* **2002**, *14*, 2171.
(26) Gorecki, W.; Andreani, R.; Berthier, C.; Armand, M.; Mali, M.; Roos, J.; Brinkmann, D. NMR, DSC, and conductivity study of a poly(ethylene oxide) complex electrolyte: PEO($LiClO_4$)$_x$, *Sol. St. Ionics* **1986**, *18-19*, 295.
(27) Muller-Plathe, F.; vanGunsteren, W. F. Computer simulation of a polymer electrolyte: Lithium iodide in amorphous poly(ethylene oxide), *J. Chem. Phys.* **1995**, *103*, 4745.
(28) Thompson, A. P.; Heffelfinger, G. S. Direct molecular simulation of gradient-driven diffusion of large molecules using constant pressure, *J. Chem. Phys.* **1999**, *110*, 10693.
(29) Philpott, M. R.; Goliney, I. Y.; Lin, T. T. Molecular dynamics simulation of water in a contact with an iron pyrite FeS_2 surface, *J. Chem. Phys.* **2004**, *120*, 1943.
(30) Xiang, H.-Q.; Tanaka, K.; Takahara, A.; Kajiyama, T. Spectroscopic and Electrochemical Characterizations of Dilithium Octacyanophthalocyanine Langmuir-Blodgett films, *Langmuir* **2002**, *18*, 2223.